

Adaptive liquid microlenses activated by stimuli-responsive hydrogels

Liang Dong¹, Abhishek K. Agarwal¹, David J. Beebe² & Hongrui Jiang¹

Despite its compactness, the human eye can easily focus on different distances by adjusting the shape of its lens with the help of ciliary muscles¹. In contrast, traditional man-made optical systems achieve focusing by physical displacement of the lenses used. But in recent years, advances in miniaturization technology have led to optical systems that no longer require complicated mechanical systems to tune and adjust optical performance. These systems have found wide use in photonics, displays and biomedical systems. They are either based on arrays of microlenses with fixed focal lengths^{2–5}, or use external control to adjust the microlens focal length^{6–12}. An intriguing example is the tunable liquid lens, where electrowetting or external pressure manipulates the shape of a liquid droplet and thereby adjusts its optical properties. Here we demonstrate a liquid lens system that allows for autonomous focusing. The central component is a stimuli-responsive hydrogel¹³ integrated into a microfluidic system and serving as the container for a liquid droplet, with the hydrogel simultaneously sensing the presence of stimuli and actuating adjustments to the shape—and hence focal length—of the droplet. By working at the micrometre scale where ionic diffusion and surface tension scale favourably¹⁴, we can use pinned liquid–liquid interfaces to obtain stable devices and realize response times of ten to a few tens of seconds. The microlenses, which can have a focal length ranging from $-\infty$ to $+\infty$ (divergent and convergent), are also readily integrated into arrays that may find use in applications such as sensing, medical diagnostics and lab-on-a-chip technologies^{15–19}.

In our system, we use the meniscus between water and oil as an optical lens and adjust its focal length by changing the curvature of this meniscus (Supplementary Video 1). The basic design (Fig. 1) consists of a stimuli-responsive hydrogel ring placed within a microfluidic channel system, and sandwiched between a glass plate and an aperture slip, the latter with an opening centred over the ring. The microchannels are filled with water, and oil is placed on top of this structure and capped with a glass cover slip (Methods). The sidewall and bottom surface of the aperture ('ca' in Fig. 1b) are hydrophilic and the top surface ('ts' in Fig. 1b) is hydrophobic, which ensures that the water–oil meniscus is pinned along the hydrophobic–hydrophilic contact line 'ca–ts' (that is, the top edge of the aperture opening). When exposed to an appropriate stimulus (which could be pH²⁰, temperature²⁰, light^{21,22}, an electric field²³, antigens²⁴, and so on), the hydrogel ring underneath the aperture opening responds by expanding or shrinking, owing to the absorption or release of water via the hydrogel network interstitials¹³; this leads to a change in the volume of the water droplet located in the middle of the ring. The net volume changes—the change in the volume enclosed by the ring, and the change in water droplet volume—cause a change in the pressure difference P across the water–oil interface, with P directly determining the geometry of the liquid meniscus. Because the contact line of the meniscus is pinned and stationary, volume

changes are translated into a change in curvature and hence angle θ (Fig. 1b), which determines the focal length of the microlens. Angle θ may attain any value in the interval $-(90^\circ - \theta_\beta) \leq \theta \leq \theta_\alpha$ by varying P (Supplementary Information), where θ_α and θ_β are the water contact angles on the 'ts' and 'ca' surfaces, respectively.

Here we use three hydrogels to produce the 'smart' attribute of the microlens, namely NIPAAm, a temperature-sensitive hydrogel, and AA and DMAEMA, which are pH-sensitive hydrogels (see Methods for details).

We first demonstrate the 'smart liquid microlens' concept with the temperature-sensitive NIPAAm hydrogel that expands at low temperatures and contracts at high temperatures, with a volume transition temperature of approximately 32 °C (Fig. 2 and Supplementary Information; see Methods for details on device fabrication). In this system, a polymer jacket placed around the hydrogel ring physically restricts the latter's movement so that it expands and contracts only at its inside periphery (Fig. 2b, c). At low temperatures, the liquid meniscus grows because the volume increase of the hydrogel upon expansion is larger than the volume of water lost from the ring due to absorption by the hydrogel; at high temperatures, the

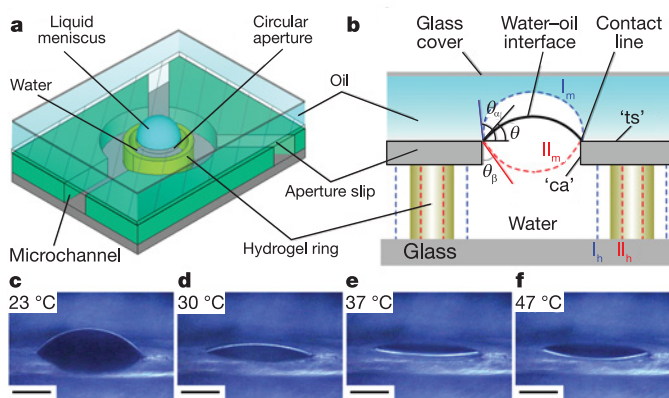


Figure 1 | Smart microlens using a pinned liquid–liquid interface. **a**, The water–oil interface forms the liquid microlens. The microchannels allow the flow of fluids to the microlens structure. **b**, Smart variable-focus mechanism. The hydrophilic sidewall and bottom surface ('ca') and hydrophobic top surface ('ts') of the aperture pin the water–oil meniscus along the contact line 'ca–ts'. The expansion and contraction of the hydrogel regulates the shape of the liquid meniscus by changing the angle θ of the pinned water–oil interface. The blue dashed lines show the expanded state of the hydrogel ring ('I_h') and the corresponding divergent microlens ('II_m') at $\theta = \theta_\alpha$. The red dashed lines show the contracted state of the hydrogel ring ('II_h') and the corresponding convergent microlens ('II_m') at $\theta = -(90^\circ - \theta_\beta)$. **c–f**, The shape of the liquid microlens varies with local environmental temperature. Scale bars, 1.0 mm.

¹Department of Electrical and Computer Engineering, ²Department of Biomedical Engineering, University of Wisconsin-Madison, Madison, Wisconsin 53706, USA.

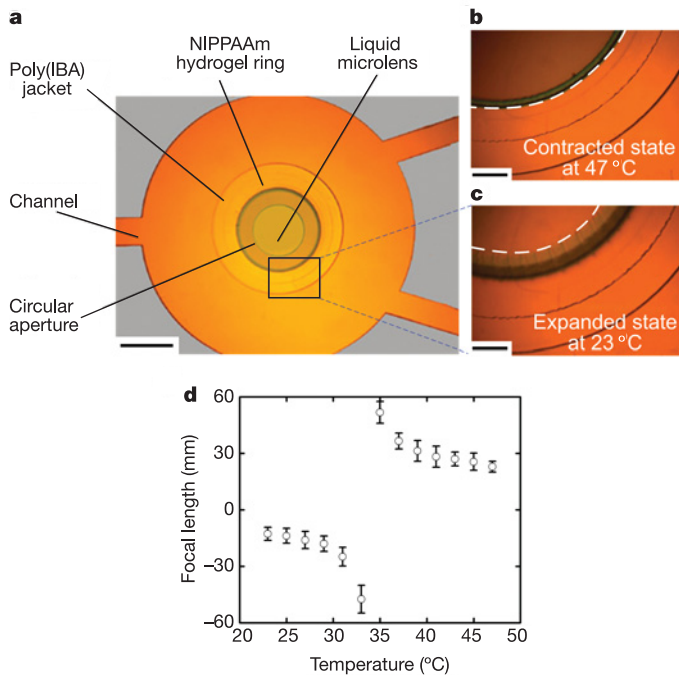


Figure 2 | A smart temperature-sensitive liquid microlens using NIPAAm hydrogel. NIPAAm, *N*-isopropylacrylamide; IBA, isobornyl acrylate; see Methods for details. **a**, An optical image of the device. Scale bar, 2.0 mm. **b**, **c**, The contracted (**b**) and expanded (**c**) states of the hydrogel ring. The dashed lines show the boundaries of the inside periphery of the hydrogel ring at two temperature states. Scale bars, 500 μm . **d**, The focal length of the microlens as a function of temperature. The microlens is divergent between 23 °C (focal length = -11.7 mm) and 33 °C (focal length approaches $-\infty$). Between 33 °C and 47 °C, the microlens becomes convergent with a positive focal length from $+\infty$ to 22.8 mm. Error bars, \pm s.d.

liquid meniscus retreats because the water release accompanying hydrogel shrinkage is unable to compensate for the decrease in physical volume of the hydrogel ring (see Supplementary Fig. S1). The difference between the physical volume change of the hydrogel and the volume change in water outside the hydrogel is probably due to the different amount and structure of bound and free water within a swollen and collapsed hydrogel²⁵. Figure 2d shows how the microlens adjusts its focal length from several millimetres to infinity in both positive and negative regimes as the temperature varies. For characterization only, an external heater is used here to change the local environmental temperature. A response time of 20–25 s is observed for the device; this refers to the time from turning on the heater to a visual change in the shape of the liquid meniscus (including 10–15 s of heater ramp and stabilization time).

Our second smart liquid microlens is fabricated using the pH-sensitive AA hydrogel, which expands in basic solutions and contracts in acidic solutions with a volume transition point at pH 5.5 (Fig. 3 and Supplementary Information; see Methods for device fabrication). In this system, the volume of the hydrogel ring is regulated by exposing its outside periphery to various pH buffers flowing through the microchannel (Fig. 3b, c). This effect ensures that as the buffer solution's pH value increases, the meniscus bulges upward and thereby decreases the focal length of the microlens (Fig. 3d; also see Supplementary Fig. S2). This observation indicates that the ring expansion and decrease in the volume enclosed inside the ring exceeds the decrease in water volume due to the absorption of the droplet by the surrounding hydrogel ring. The response time of the pH-sensitive microlens is approximately 12 s, as judged by exposing the hydrogel ring to the desired pH buffers and measuring the time interval until a visual change in the shape of the liquid meniscus is observable. Figure 3e illustrates the ability to focus on objects at

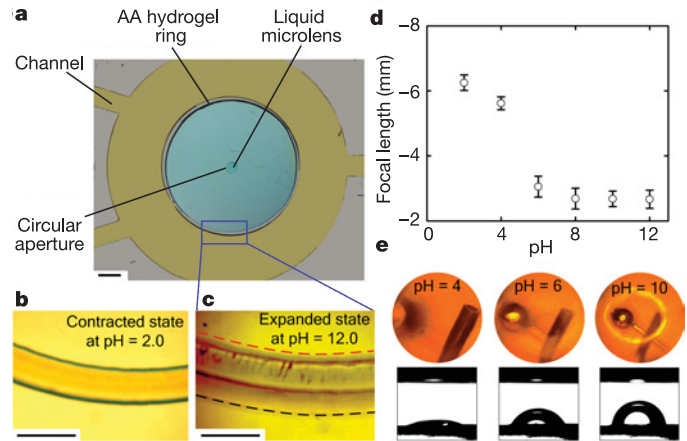


Figure 3 | A smart pH-sensitive liquid microlens using AA hydrogel. AA, acrylic acid; see Methods for details. **a**, An optical image of the device. Scale bar, 1.0 mm. **b**, The contracted state of the hydrogel ring at pH 2.0. Scale bar, 500 μm . **c**, The expanded state of the hydrogel ring at pH 12.0, where the red and black dashed lines represent the boundaries of the inside and outside periphery of the hydrogel ring, respectively. Scale bar, 500 μm . **d**, The focal length of the microlens as a function of pH. Error bars, \pm s.d. **e**, 'Smart' focusing of two objects (a ball connected to a pillar and a needle tip separated by 1.38 cm). At pH 2.0, both objects are out of focus (not shown). The top row optical images show (left to right): the needle tip is focused at pH 4.0; the focus point falls somewhere between the two objects at pH 6.0; and the ball is focused at pH 10.0. The bottom row shows the corresponding optical images of the liquid droplet itself.

different distances: the microlens device is focused on a needle tip when using a buffer solution with pH 4.0, and subsequently on a ball when changing the buffer pH to 10.0.

Inspired by insect (for example, *Drosophila*) compound eyes, where each repeating ommatidium²⁶ is responsible for one area in space and can progressively turn on and off as an object moves across the visual field of the eye, we extend the single liquid microlens to a microlens array. As a first step, we integrate two liquid microlenses in one microchannel to dynamically monitor two areas (Fig. 4 and Supplementary Information; see Methods for device fabrication). These two microlenses have identical structures, but are fabricated from two pH-sensitive hydrogels with opposite responses to pH changes: the AA hydrogel used already for the one-lens system expands at high pH and contracts at low pH, whereas DMAEMA hydrogel expands at low pH and contracts at high pH with a volume transition point of about pH 7.0. When replacing an initial high-pH buffer with a low-pH buffer, the liquid meniscus of the DMAEMA hydrogel-based microlens A gradually bulges up to move the focal plane closer to the aperture, while the AA hydrogel-based microlens B exhibits the opposite effect and moves the focal plane further away from the aperture (Fig. 4a–d and Supplementary Video 2). The object planes of microlenses A and B thus move through space perpendicular to the aperture as the focal lengths gradually change (Fig. 4e). In the array, each microlens provides information about one designated area. In this regard, the array mimics compound eyes where different unit eyes monitor different areas²⁶; but the individual liquid microlenses within our array have in addition variable-focus ability and can in principle be designed to respond to different stimuli.

The present hydrogel-based microlens system is relatively simple and highly adaptable, particularly as appropriate modifications to the fabrication procedure (for example, controlling photo-definability, crosslinking density, and porosity) should make it possible to incorporate some of the many other hydrogels^{20–24} that respond, for example, to light, electric fields and antigens. This should make it possible to incorporate microlenses controlled by different hydrogels into functionally complex arrays, which might then find use as physical, biological or chemical sensors that are capable of sensing

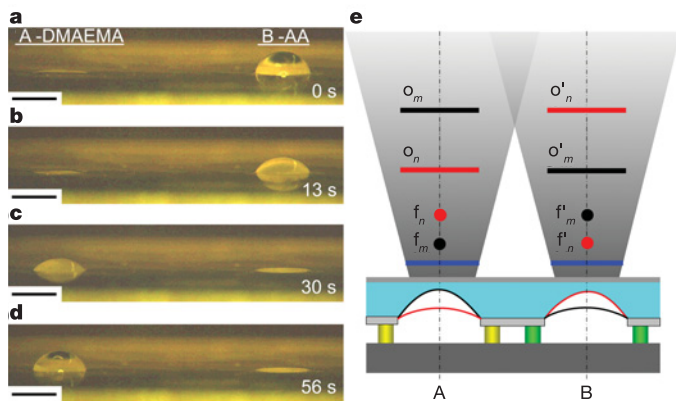


Figure 4 | Combination of two smart pH-sensitive liquid microlenses to monitor two areas in space. **a–d**, Optical images of the operation of the two-pixel pH-sensitive liquid microlens array, showing snapshots at indicated times. Left, microlens A, 2-(dimethylamino)ethyl methacrylate (DMAEMA); right, microlens B, AA. Scale bars, 500 μm . **e**, Conceptual diagram showing the monitoring of different areas in space by lenses A and B. The blue lines represent the image planes. The red and black curves represent the oil–water interfaces of the two microlenses at two pH values, n and m , respectively. For microlens A, the focal point changes from f_n (red point) to f_m (black point) and the object plane moves from O_n (red line) to O_m (black line), as the pH value of its surrounding fluid changes from n to m . Microlens B exhibits opposite effects (f'_n to f'_m and O'_n to O'_m) when simultaneously exposed to this same local environmental fluid.

multiple environmental parameters and generating optical outputs or visible images that are simple to read. The versatility of this system, together with the simple and direct sensing and read-out mechanisms, also mean that the hydrophobic–hydrophilic boundary interface at the ‘heart’ of the device can contain an aperture opening of an arbitrary shape (see Supplementary Fig. S3 for a cylindrical liquid microlens with a rectangular aperture). Moreover, the interface can be realized with a variety of substrates (for example, glass or polymers), with no strict geometrical substrate requirements. This should allow the fabrication of three-dimensional microlens arrays on flexible polymer substrates²⁷, and thus the achievement of larger fields of view (see Supplementary Fig. S4 for a liquid microlens array on a curved surface).

A number of alternative microlens technologies allow for simple and cheap fabrication of small devices with fast response times (in the millisecond regime). The present hydrogel-based systems are much slower, but further miniaturization of the hydrogel structures²⁸ should improve the response times at least somewhat. Nonetheless, a unique feature of these systems is that they do not require complicated external control systems; instead, the microlenses can autonomously respond to changes intrinsic to a liquid sample being studied and provide visible output signals. Another attractive feature is that these microlenses can be readily integrated with existing electronic and opto-electronic systems (for example, simple planar electrodes can be used to precisely modulate the volumetric changes of an electrically responsive hydrogel²⁹), with lens fabrication by *in situ* liquid-phase photopolymerization²⁸ facilitating the integration with existing microfluidic components³⁰. It should therefore be not too difficult to produce functionally complex yet relatively simple systems—for example, diagnostic or lab-on-a-chip applications.

METHODS

Photopolymerizable mixtures. The NIPAAm temperature-sensitive hydrogel prepolymer mixture consists of *N*-isopropylacrylamide (NIPAAm), *N,N'*-methylenebisacrylamide, dimethyl sulphoxide, deionized water and 2,2-dimethoxy-2-phenylacetophenone (DMPA) in the weight ratio of 2.18:0.124:3.0:1.0:0.154. The AA pH-sensitive hydrogel prepolymer mixture consists of acrylic acid (AA), 2-hydroxyethyl methacrylate (HEMA, 0–50 p.p.m. MEHQ inhibitor), ethylene glycol dimethacrylate (EGDMA) and DMPA in

the weight ratio of 4.054:29.286:0.334:1.0. The DMAEMA pH-sensitive hydrogel pre-polymer mixture consists of 2-(dimethylamino)ethyl methacrylate (DMAEMA), HEMA, EGDMA and DMPA in the weight ratio of 5.718:27.627:0.467:1.0. The microchannels and aperture slips of all devices, and the polymer jacket in Fig. 2, are made by photopatterning a non-responsive prepolymer mixture (called poly(IBA)) consisting of isobornyl acrylate (IBA), tetraethylene glycol dimethacrylate and DMPA in the weight ratio of 31.66:1.66:1.0.

Fabrication of devices. The devices in Figs 2–4 are fabricated by using liquid-phase photopolymerization (LP³) based on ultraviolet (UV) photolithography²⁸. The fabrication starts with a 250- μm -thick polycarbonate cartridge (HybriWells, Grace Bio-Labs) that is filled with the poly(IBA) prepolymer mixture. An aperture is formed inside the cartridge via direct photopatterning of the mixture through a photomask aligned on top of the cartridge (UV intensity $I_{\text{UV,poly(IBA)}} = 7.7 \text{ mW cm}^{-2}$; exposure time $t_{\text{UV,poly(IBA)}} = 24 \text{ s}$). The cartridge's thin liner is peeled off, leaving one side of the photopatterned poly(IBA) slip exposed to the ambient air. 100% ethanol is used to remove the unpolymerized pre-polymer. To make the poly(IBA) sidewall of the aperture hydrophilic, oxygen plasma treatment is carried out using a reactive ion etching system (Technics Micro-RIE series 800-IIC; power supply 70 W at 13.56 MHz; oxygen flow rate 3.0 $\text{cm}^3 \text{ STP min}^{-1}$; gas pressure 107 mtorr; treatment time 40 s). Next, a cavity is formed by adhering the treated surface of the poly(IBA) slip to the glass substrate surface using double-sided adhesive spacer tapes along the edge of the slip. The cavity height is determined by the thickness of the adhesive tapes (750 μm and 250 μm for the microlenses in Fig. 2 and Figs 3–4, respectively). The poly(IBA) microchannels and jackets are constructed inside the cavity by using a sequential step-and-repeat LP³ process ($I_{\text{UV,poly(IBA)}} = 8.5 \text{ mW cm}^{-2}$ and $t_{\text{UV,poly(IBA)}} = 34.5 \text{ s}$). The polycarbonate cartridge cover is finally peeled off of the poly(IBA) aperture slip, which now serves as the top slip of the microchannels.

The NIPAAm hydrogel ring (Fig. 2) and AA hydrogel ring (Figs 3–4) are constructed by photopatterning the corresponding aforementioned hydrogel liquid prepolymer mixtures. The photolithography conditions are: $I_{\text{UV,NIPAAm}} = 12.5 \text{ mW cm}^{-2}$ and $t_{\text{UV,NIPAAm}} = 8.5 \text{ s}$; $I_{\text{UV,AA}} = 10 \text{ mW cm}^{-2}$ and $t_{\text{UV,AA}} = 45.3 \text{ s}$. Next, the DMAEMA hydrogel ring (Fig. 4), which has an identical structure to its neighbouring AA hydrogel ring using the sequential step-and-repeat LP³ process ($I_{\text{UV,DMAEMA}} = 19.0 \text{ mW cm}^{-2}$ and $t_{\text{UV,DMAEMA}} = 50 \text{ s}$). The top-side surface of the aperture slip is rendered hydrophobic by manually coating it with an octadecyltrichlorosilane solution diluted by hexadecane (0.2 vol.%). A liquid meniscus is initially formed by manually loading water into the hydrogel ring through the aperture. The initial curvature of the meniscus depends on the amount of the loaded water. To store the oil on top of the water, a pre-fabricated fence made of polydimethylsiloxane elastomer is adhered to the aperture slip. The fence is then capped by a 100- μm -thick glass cover slip.

Received 23 December 2005; accepted 23 June 2006.

- Toates, F. M. Accommodation function of human eye. *Physiol. Rev.* **52**, 828–863 (1972).
- Popovic, Z. D., Sprague, R. A. & Connell, G. A. N. Technique for monolithic fabrication of microlens arrays. *Appl. Opt.* **27**, 1281–1284 (1988).
- Cayre, O. J. & Pounov, V. N. Fabrication of microlens arrays by gel trapping of self-assembled particle monolayers at the decane–water interface. *J. Mater. Chem.* **14**, 3300–3302 (2004).
- Yang, R., Wang, W. J. & Soper, S. A. Out-of-plane microlens array fabricated using ultraviolet lithography. *Appl. Phys. Lett.* **86**, 161110 (2005).
- Yang, S. *et al.* Functional biomimetic microlens arrays with integrated pores. *Adv. Mater.* **17**, 435–438 (2005).
- Zhang, D. Y., Lien, V., Berdichevsky, Y., Choi, J. & Lo, Y. H. Fluidic adaptive lens with high focal length tunability. *Appl. Phys. Lett.* **82**, 3171–3172 (2003).
- Saitoh, A. & Tanaka, K. Self-developing aspherical chalcogenide-glass microlenses for semiconductor lasers. *Appl. Phys. Lett.* **83**, 1725–1727 (2003).
- Hayes, R. A. & Feenstra, B. J. Video-speed electronic paper based on electrowetting. *Nature* **425**, 383–385 (2003).
- Kuiper, S. & Hendriks, B. H. W. Variable-focus liquid lens for miniature cameras. *Appl. Phys. Lett.* **85**, 1128–1130 (2004).
- Ren, H. W., Fan, Y. H. & Wu, S. T. Liquid-crystal microlens arrays using patterned polymer networks. *Opt. Lett.* **29**, 1608–1610 (2004).
- Lopez, C. A., Lee, C. C. & Hirs, A. H. Electrochemically activated adaptive liquid lens. *Appl. Phys. Lett.* **87**, 134102 (2005).
- Ren, H. & Wu, S. T. Variable-focus liquid lens by changing aperture. *Appl. Phys. Lett.* **86**, 211107 (2005).
- Osada, Y., Gong, J. P. & Tanaka, Y. Polymer gels. *J. Macromol. Sci. C* **44**, 87–112 (2004).
- Atencia, J. & Beebe, D. J. Controlled microfluidic interfaces. *Nature* **437**, 648–655 (2005).

15. Camou, S., Fujita, H. & Fujii, T. PDMS 2D optical lens integrated with microfluidic channels: Principle and characterization. *Lab Chip* **3**, 40–45 (2003).
16. Chronis, N., Liu, G. L., Jeong, K. H. & Lee, L. P. Tunable liquid-filled microlens array integrated with microfluidic network. *Opt. Express* **11**, 2370–2378 (2003).
17. Burns, M. A. *et al.* An integrated nanoliter DNA analysis device. *Science* **282**, 484–487 (1998).
18. Choi, H. W. *et al.* GaN micro-light-emitting diode arrays with monolithically integrated sapphire microlenses. *Appl. Phys. Lett.* **84**, 2253–2255 (2004).
19. Carlson, K. *et al.* *In vivo* fiber-optic confocal reflectance microscope with an injection-molded plastic miniature objective lens. *Appl. Opt.* **44**, 1792–1797 (2005).
20. Park, T. G. & Hoffman, A. S. Synthesis and characterization of pH- and temperature-sensitive hydrogels. *J. Appl. Polym. Sci.* **46**, 659–671 (1992).
21. Suzuki, A. & Tanaka, T. Phase transition in polymer gels induced by visible light. *Nature* **346**, 345–347 (1990).
22. Sershen, S. R. *et al.* Independent optical control of microfluidic valves formed from optomechanically responsive nanocomposite hydrogels. *Adv. Mater.* **17**, 1366–1368 (2005).
23. Tanaka, T., Nishio, I., Sun, S. T. & Uenonishio, S. Collapse of gels in an electric field. *Science* **218**, 467–469 (1982).
24. Miyata, T., Asami, N. & Uragami, T. A reversibly antigen-responsive hydrogel. *Nature* **399**, 766–769 (1999).
25. Lele, A. K., Hirve, M. M., Badiger, M. V. & Mashelkar, R. A. Predictions of bound water content in poly(*N*-isopropylacrylamide) gel. *Macromolecules* **30**, 157–159 (1997).
26. Land, M. F. Visual acuity in insects. *Annu. Rev. Entomol.* **42**, 147–177 (1997).
27. Jacobs, H. O., Tao, A. R., Schwartz, A., Gracias, D. H. & Whitesides, G. M. Fabrication of a cylindrical display by patterned assembly. *Science* **296**, 323–325 (2002).
28. Beebe, D. J. *et al.* Functional hydrogel structures for autonomous flow control inside microfluidic channels. *Nature* **404**, 588–590 (2000).
29. Bassetti, M. J., Chatterjee, A. N., Aluru, N. R. & Beebe, D. J. Development and modeling of electrically triggered hydrogels for microfluidic applications. *J. Microelectromech. Syst.* **14**, 1198–1207 (2005).
30. Agarwal, A. K., Sridharamurthy, S. S., Beebe, D. J. & Jiang, H. Programmable autonomous micromixers and micropumps. *J. Microelectromech. Syst.* **14**, 1409–1421 (2005).

Supplementary Information is linked to the online version of the paper at www.nature.com/nature.

Acknowledgements This research was supported in part by the US Department of Homeland Security, through a grant awarded to the National Center for Food Protection and Defense at the University of Minnesota, and in part by the Wisconsin Alumni Research Foundation (WARF). The authors thank J. Moorthy and S.S. Sridharamurthy for discussions.

Author Information Reprints and permissions information is available at npg.nature.com/reprintsandpermissions. The authors declare no competing financial interests. Correspondence and requests for materials should be addressed to H.J. (hongrui@engr.wisc.edu).